JCTC Journal of Chemical Theory and Computation

pubs.acs.org/JCTC Article

Combining Time-Dependent Density Functional Theory and the ΔSCF Approach for Accurate Core-Electron Spectra

Marcus Annegarn, Juhan Matthias Kahk, and Johannes Lischner*

Cite This: J. Chem. Theory Comput. 2022, 18, 7620−7629 Read Online

ACCESS | Metrics & More | Article Recommendations | Supporting Information

ABSTRACT: Spectroscopies that probe electronic excitations from core levels into unoccupied orbitals, such as X-ray absorption spectroscopy and electron energy loss spectroscopy, are widely used to gain insight into the electronic and chemical structure of materials. To support the interpretation of experimental spectra, we assess the performance of a first-principles approach that combines linear-response time-dependent density (TDDFT) functional theory with the Δ self-consistent field (ΔSCF) approach. In particular, we first use TDDFT to calculate the core-level spectrum and then shift the spectrum such that the lowest excitation energy from TDDFT agrees with that from ΔSCF. We apply this method to several small molecules and find encouraging agreement between calculated and measured spectra.

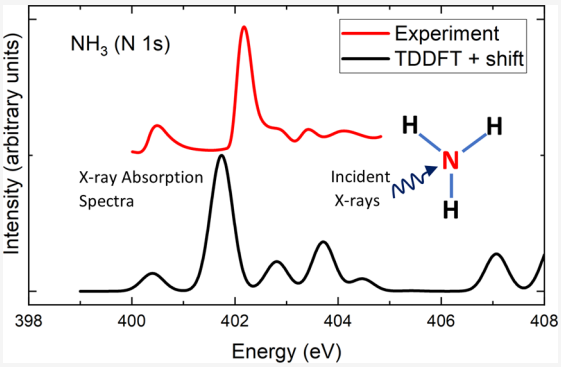

INTRODUCTION

X-ray absorption spectroscopy (XAS) and electron energy loss spectroscopy (EELS) are powerful and widely used characterization techniques that can provide information about the elements present in a sample as well as their chemical environments. For example, these techniques have been used for studying the electronic structure of functional materials,[1,2] probing the chemical bonding in systems such as water and ice[3,4] or analyzing the properties of pollution particles.[5,6]

Both XAS and EELS measure energies of electronic excitations from core levels into unoccupied states. The onset of the spectrum corresponding to transitions from 1s core states into the lowest unoccupied orbitals is called the K-edge, while the L-edge indicates the onset of transitions from core states with a principal quantum number of $n = 2$. While it is usually straightforward to use XAS and EELS for elemental analysis of samples, the identification of specific chemical environments can be more challenging. In principle, the assignment of chemical environments should be possible by comparing the measured spectrum to a set of experimental reference spectra. In practice, however, obtaining reliable reference spectra for a broad range of chemical environments is often not straightforward.

Alternatively, it is possible to obtain reference spectra from first-principles calculations. For example, linear-response time-dependent density functional theory (TDDFT)[7] has been widely used to predict core-excitation energies and intensities of XAS spectra.[8−11] Core spectra from TDDFT often accurately reproduce the qualitative shape of measured spectra, but absolute core-level excitation energies are not quantitatively reproduced with errors of several electronvolts.[12−14] This shortcoming of standard TDDFT calculations is a consequence of approximate exchange within the exchange−correlation functionals.[15] In particular, many standard exchange−correlation potentials exhibit an incorrect asymptotic behavior both far away and very close to the atomic nuclei.[16] Often, good quantitative agreement with the experiment can be obtained by subtracting a constant energy shift from all excitation energies, with the value of the shift being determined empirically by comparison to the experiment.[17] However, this post hoc calibration of the calculated TDDFT spectrum can be problematic in complex materials containing many different chemical environments. In such cases, it is often desirable to calculate accurate absolute core-electron excitation energies and avoid the need for empirical shifts.

Accurate absolute core-level excitation energies have recently been obtained using the Δ self-consistent-field (ΔSCF) approach[18−20] in which the excitation energy is determined as a total energy difference between the ground state and the state with a core hole. For transitions from core orbitals to the vacuum level, which are probed in X-ray photoemission experiments, some of us recently demonstrated that highly accurate excitation energies (also known as core-level binding energies (BEs)) can be obtained for molecules, solids, and surfaces when the SCAN exchange−correlation

Received: August 9, 2022
Published: November 16, 2022

https://doi.org/10.1021/acs.jctc.2c00817
J. Chem. Theory Comput. 2022, 18, 7620−7629

functional is used in conjunction with an accurate treatment of relativistic effects.[21,22] The ΔSCF approach has also been used to determine K-edge energies (KEs) and energies of higher-lying excited states by calculating the total energy difference of the ground state and a state in which one core electron has been promoted to an unoccupied state.[23,24] For these neutral excitations, convergence difficulties associated with a variational collapse are often encountered.[24] To overcome this problem, Hait and Head-Gordon used a square gradient minimization approach and obtained good agreement with experiment for a set of molecular compounds.[25,26] However, the determination of spectra with this approach is less straightforward as a separate calculation is required for each excited state (in contrast to linear-response TDDFT, which yields all excitation states in a single shot).

Other approaches for simulating core-electron spectra are based on Kohn–Sham eigenvalues,[27,28] the coupled cluster approach,[29] Slater transition-state theory,[30] and the GW/BSE approach.[31,32] Finally, machine learning techniques have been developed to predict the spectra of complex materials, but these techniques also need accurate reference spectra to construct the training data set.[33−36]

A simple alternative approach to obtain core-level spectra is to combine ΔSCF approach with linear-response TDDFT:[37] instead of using experimental data to determine the energy shift that is applied to the TDDFT spectrum, one determines this shift from first-principles using a ΔSCF calculation of the lowest excited state. In this paper, we apply this approach to a set of molecules and assess its accuracy by comparing the calculated spectra to experimental results. For most systems, we find good quantitative agreement when appropriate exchange–correlation functionals are used. It is straightforward to apply this method to more complex systems, such as surfaces or clusters.

METHODS

The core-level spectra are obtained from

$$S(\omega) = \sum_I f_I L^{(\eta)}(\hbar\omega - E_I) \tag{1}$$

with ω denoting the light frequency, f_I is the oscillator strength of the Ith excited state, and $L^{(\eta)}$ denotes a Lorentzian with a full width at half-maximum (FWHM) of η. Also, E_I is the energy of the Ith excited state and obtained via

$$E_I = E_I^{\mathrm{TDDFT}} + \Delta \tag{2}$$

where E_I^{TDDFT} are the excitation energies obtained from TDDFT and Δ denotes a constant energy shift that is applied to all excitation energies. The shift is given by

$$\Delta = E_1^{\Delta\mathrm{SCF}} - E_1^{\mathrm{TDDFT}} \tag{3}$$

with $I = 1$ referring to the lowest excitation and $E_1^{\Delta\mathrm{SCF}}$ denotes the corresponding excitation energy obtained from ΔSCF.

For example, Table 1 shows the lowest neutral excitation energy of NH_3 calculated with TDDFT using different exchange–correlation functionals (BHLYP, BLYP, PBE0, and Hartree–Fock (HF)). The calculated results differ from the experimental value at least by several electronvolts. In contrast, the ΔSCF results for all exchange–correlation functionals are in very good agreement with experiment.

In the following, we describe in more detail how the ΔSCF calculations and the linear-response TDDFT calculations are carried out. For all molecules, calculations were carried out for the relaxed structure obtained using the SCAN functional with the default tight basis sets in the FHI-AIMS computer program.[39,40]

Table 1. Comparison of K-Edge Energies of NH_3 from TDDFT and the ΔSCF Approaches for Different Exchange–Correlation Functionals[a]

	BHLYP (eV)	BLYP (eV)	PBE0 (eV)	HF (eV)	exp. (eV)
TDDFT	398.7	379.9	389.1	416.0	400.4
ΔSCF	400.4	400.5	400.6	400.5	400.4

[a]The experimental result is taken from ref 38. Computational details are described in the ΔSCF Approach and Time-Dependent Density Functional Theory sections.

ΔSCF Approach. In the ΔSCF approach, excitation energies are obtained as total energy differences between the relevant excited states and the ground state. For example, core-electron binding energies measured in X-ray photoelectron spectroscopy (XPS) can be obtained by subtracting the ground-state energy of the neutral system from the total energy of the system with a core hole, which is obtained by minimizing the total energy under the constraint that a given core orbital remains unoccupied. Similarly, the lowest neutral core-electron excitation energy, which is measured in XAS or EELS, can be obtained by calculating the total energy of the system with a core hole and an extra electron in the lowest unoccupied orbital and subtracting this from the ground-state energy (without a core hole). We stress that a separate ΔSCF calculation is required for each core-electron binding energy and each core-electron excitation energy.

The ΔSCF calculations were performed using the FHI-AIMS computer program,[39,40] an all-electron code that uses localized basis sets defined on a grid of points in real space. We include relativistic effects using the scaled zeroth-order regular approximation (ZORA).[39,41−44] All molecules in this study are closed shell, but spin polarization is included in the calculations with a core hole. It has been pointed out that the ΔSCF approach cannot properly model singlet excitations as those cannot be described by a single Slater determinant.[25] Despite this shortcoming, we find below that the ΔSCF approach produces accurate K-edge energies—likely because the coupling between the core hole and the excited electron is weak.

The basis sets used are those described in refs 21 and 22, which are modifications of the default tight FHI-AIMS basis sets with additional basis functions for the core states. These additional functions allow us to describe the contraction of the occupied 1s state in the presence of a core hole. The following five different exchange–correlation functionals were tested: SCAN, BHLYP, BLYP, PBE0, PBE, and B3LYP. We stress that the same computational parameters (such as basis set and exchange–correlation functional) must be used in both the ground-state and the excited-state calculation to obtain accurate excitation energies. Particular care must be taken when the molecules contain atoms in equivalent sites. In this case, additional strategies for localizing the core holes on a desired atom must be employed, as explained in ref 22.

Time-Dependent Density Functional Theory. We also carry out linear-response TDDFT calculations of excited states involving transitions from core orbitals to unoccupied states using the NWChem program package.[45] For this, we ignore (or "freeze") transitions from all occupied states with energies

https://doi.org/10.1021/acs.jctc.2c00817
J. Chem. Theory Comput. 2022, 18, 7620−7629

exceeding that of the core orbital under consideration. This significantly reduces the computational cost of the calculations. We have verified that the inclusion of these states only leads to very small changes in the excitation energies.

We have also studied the dependence of the TDDFT spectra on the basis set and the exchange−correlation functional. Figure 1 compares the calculated spectra of the NH_3 molecule

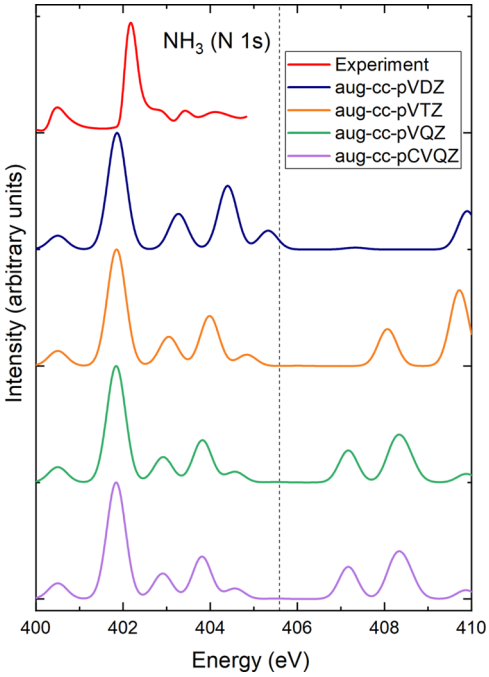

Figure 1. Comparison of measured XAS spectrum from ref 38 and TDDFT results with different basis sets for NH_3. The calculated spectra were obtained with the BHLYP functional and shifted such that the energy of the first excited state from TDDFT agrees with the BHLYP ΔSCF result. The dashed vertical line indicated the calculated ionization potential.

obtained using the BHLYP functional for different basis sets ranging from double ζ to quadruple ζ of the augmented correlation-consistent polarized, valence aug-cc-pVXZ Dunning family with X = D, T, or Q[46,47] taken from the basis set exchange.[48−50] In addition, we tested the aug-cc-pCVQZ basis, which contains additional core basis functions. For the energy range in which experimental data is available, all basis sets give similar results. Clear differences can be observed at higher excitation energies. Finally, we also compare spectra with and without the Tamm−Dancoff approximation and found almost no difference. For all TDDFT calculations in this paper, we use the aug-cc-pVQZ basis and the Tamm−Dancoff approximation.

Figure 2 compares the experimental spectrum of NH_3 and H_2O to calculated spectra obtained from different exchange−correlation functionals (BHLYP, HF, PBE0, BLYP, PBE, and B3LYP—no results for the SCAN functional were carried out as this functional is not yet available for TDDFT calculations with the NWChem code). Good agreement is found between the BHLYP result and experiment, while significant qualitative differences can be observed for the other functionals. All TDDFT calculations in the paper are therefore performed with the BHLYP functional.

RESULTS AND DISCUSSION

K-Edge Energies of Molecular Compounds. We have calculated the lowest core-electron excitation energies corresponding to transitions from atomic 1s orbitals to molecular lowest unoccupied molecular orbital (LUMO) states (also known as the K-edge energy) as well as the core-electron binding energies of a set of small molecules containing the elements H, C, N, O, and F using the ΔSCF approach. In particular, we carry out calculations for CH_4, H_2O, NH_3, HF, ethanol, acetone, CO, OCS, formaldehyde, C_2H_2, C_2H_4, and azabenzenes. All results are shown in Figure 3 and summarized in Table 2. All relevant data used to generate these graphs, as well as the experimental references, are provided in the Appendix. Atomic geometries of all molecules are provided in the Supporting Information.

Figure 3a,b compares the K-edge energies and core-electron binding energies of carbon atoms in the molecular compounds obtained with different exchange−correlation functionals. Table 2 shows that the BHLYP functional performs best for the core-electron binding energies with a mean absolute error (MAE) of 0.11 eV, while the other hybrid functionals perform somewhat worse. Regarding the semilocal functionals, SCAN performs best with an MAE of 0.15 eV, while PBE and BLYP have MAEs of 0.22 and 0.29 eV, respectively. For the K-edge energies, PBE0 performs best with an MAE of 0.24 eV. B3LYP and BLYP (both with an MAE of 0.29 eV) as well as BHLYP (0.29 eV) and PBE (0.30 eV) perform similarly, with SCAN showing the highest MAE of 0.38 eV. The origin of this large MAE for SCAN can be traced to its performance for carbon monoxide with an absolute error of 0.9 eV, while other functionals have errors of only 0.1 eV for this system. Overall, we find that the MAEs for the lowest neutral excitations tend to be somewhat higher than for the core-electron binding energies.

Figure 3c,d shows the corresponding results for oxygen atoms. Table 2 shows that among the semilocal functionals, SCAN performs best for the core-electron binding energies with an MAE of 0.21 eV. For the K-edge energies, the accuracy of SCAN is somewhat worse with an MAE of 0.32 eV, which is similar to BLYP with an MAE of 0.30 eV. Somewhat better results for the K-edge energies can be obtained with hybrid functionals. In particular, BHLYP yields an MAE of only 0.23 eV, while the MAEs of B3LYP and PBE0 are 0.32 and 0.48 eV, respectively.

Finally, Figure 3e,f shows the corresponding results for nitrogen atoms. For the core-electron binding energies, BLYP (MAE of 0.14 eV), SCAN (MAE of 0.16 eV), and BHLYP (MAE of 0.18 eV) perform best. For the K-edge energies, SCAN performs best with an MAE of 0.16 eV. BLYP, PBE, and BHLYP all show MAEs of 0.26 eV. B3LYP and PBE0 perform worst with MAEs of 0.4 and 0.38 eV, respectively.

In summary, we find that the BHLYP functional yields the most accurate K-edge energies with an overall MAE of 0.25 eV for the set of molecules studied in this work. Its performance for core-electron binding energies (MAE of 0.19 eV) is even better, and only the SCAN functional yields slightly better results with an MAE of 0.16 eV. Somewhat surprisingly, SCAN performs significantly worse for K-edge energies with an MAE of 0.33 eV.

It is interesting to correlate the performance of K-edge energies to the treatment of exchange in the different functionals. The best-performing functional BHLYP has a

https://doi.org/10.1021/acs.jctc.2c00817
J. Chem. Theory Comput. 2022, 18, 7620−7629

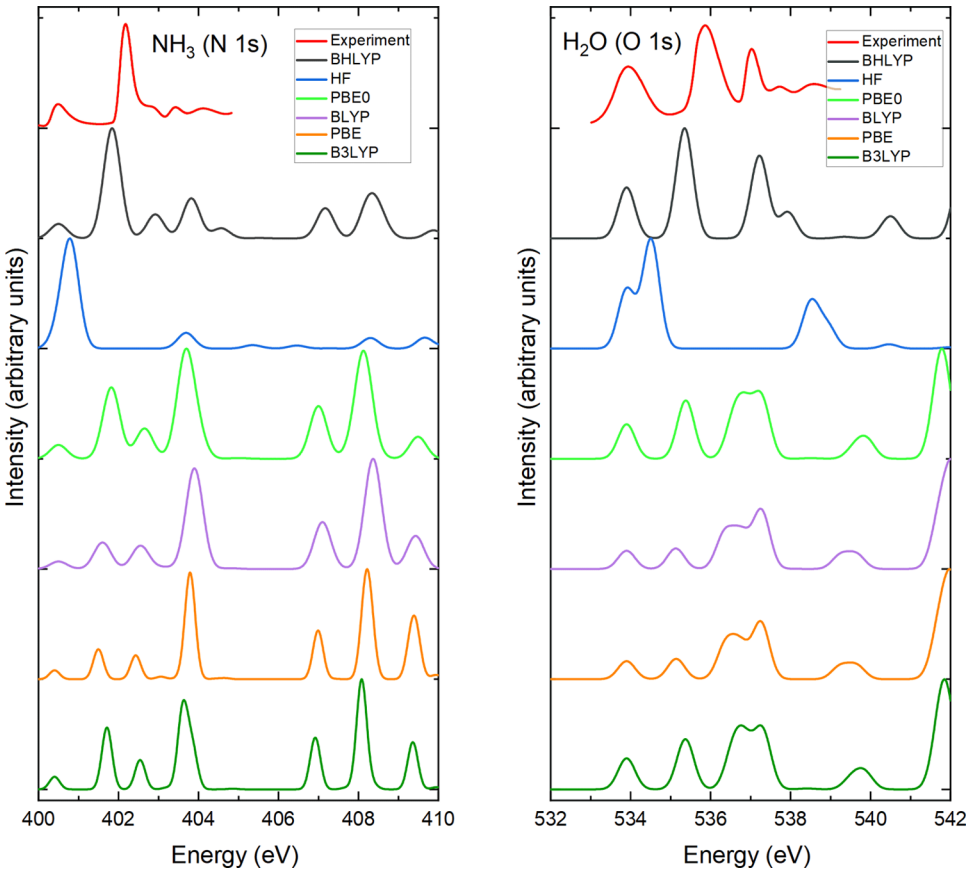

Figure 2. Comparison of the measured XAS spectrum from ref 38 and TDDFT results with different exchange−correlation functionals for NH_3 and H_2O. The calculated spectra were shifted such that the energy of the first excited state agrees with the measured value.

fraction of 50% exact exchange, while functionals with smaller fractions of exact exchange (such as PBE0 with an exact exchange fraction of 0.25 and B3LYP with a fraction of 0.2) give worse results. The need for a large fraction of exact exchange for obtaining accurate core-electron energies is consistent with the observation of Besley and co-workers[15] that the best TDDFT results for K-edge energies are obtained with ranged-separated hybrid functionals with an exact exchange fraction of 0.55 in the short range. We note, however, that the K-edge energies obtained from the approach of Besley and co-workers can differ from experiment by as much as 1 eV—significantly more than the results obtained from the ΔSCF approach with the BHLYP functional.

Core-Electron Spectra of Molecules. Figure 4 shows the calculated core-level spectra for a set of small molecules (HCHO, C_2H_2, C_2H_4, CH_4, NH_3, H_2O, HF) and compares them to experimental results. The experimental data has been fitted to a spline and smoothed for easier visual comparison. As described in the Methods section, each excitation is represented by a Lorentzian with a full width at half-maximum η. In Figure 4, we have used η = 0.3 eV for carbon spectra and 0.5 eV for oxygen, nitrogen, and fluorine spectra. The value of η was chosen such that the calculated spectra resemble the experimental spectra. However, the same value of η was used for all spectra of the same element.

Figure 4a compares the calculated carbon 1s XAS spectrum of formaldehyde (HCHO) with experimental data taken from ref 51. Both the experimental and the calculated spectra show a large peak near 285.5 eV. In the measured spectrum, this peak appears very broad and is split into a set of smaller subpeaks. This peak splitting has been interpreted as a vibrational effect[51] with a single electronic excitation (associated with the transition of an electron from the C 1s core level to an unoccupied π^* orbital) coupled to various vibrations associated with H−C bending and stretching as well as C−O stretching. Since the atomic nuclei are fixed in our calculations, we do not capture these vibrational effects. Following this main peak, there is an energy gap in both the experimental and the calculated spectra. At higher energies (starting at approximately 290 eV), a set of smaller peaks can be observed, which arise from transitions from the C 1s state to Rydberg states of the molecule. Overall, there is good agreement for both the positions and intensities of the peaks between the calculated and the measured spectra.

The experimental core-electron spectrum of C_2H_4 (shown in Figure 4b) is qualitatively similar to that of formaldehyde. In particular, a large peak is found at 284.7 eV which is split into two peaks because of the coupling to the symmetric C−H stretching mode. This peak arises from transitions from the carbon 1s orbital to the molecular LUMO. At energies higher than 287.7 eV, a series of smaller transitions are observed, which are attributed to transitions into Rydberg states. The calculated spectrum also exhibits a large peak whose energy is in good agreement with the experimental one as well as a series of smaller peaks at higher energies. Similarly, good agreement between theory and experiment is found for C_2H_2 (see Figure 4c).

Figure 4d compares the XAS spectrum[38] of CH_4 to the calculated result. In this case, the agreement between theory and experiment is clearly worse. It is important to note,

https://doi.org/10.1021/acs.jctc.2c00817
J. Chem. Theory Comput. 2022, 18, 7620−7629

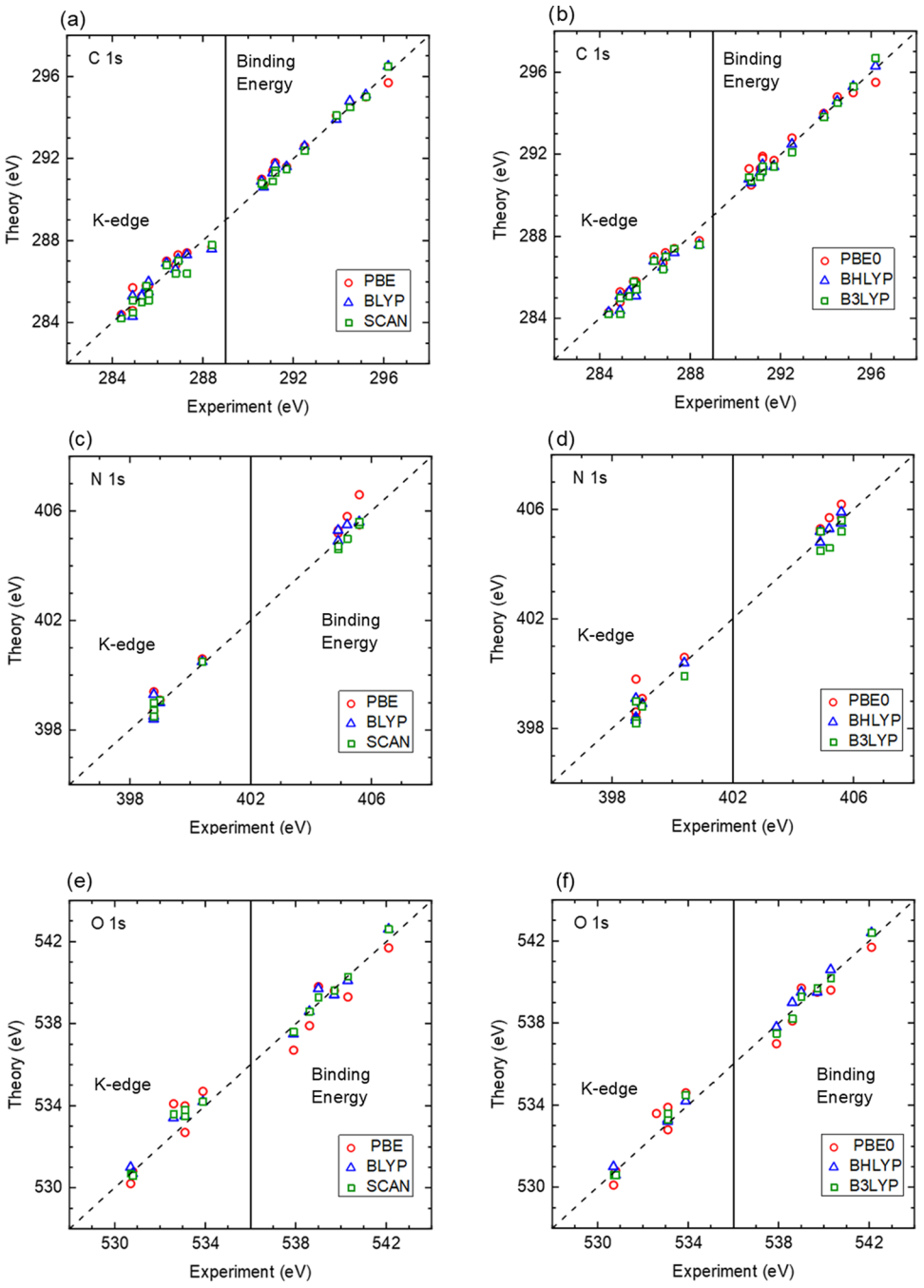

Figure 3. Comparison of calculated and measured core-electron binding energies (BEs) and K-edge energies. Results were obtained using the ΔSCF approach with different exchange−correlation functionals. The panels in the left column compare the performance of semilocal functionals (PBE, BLYP, and SCAN), and the panels in the right column compare three different hybrid functionals (PBE0, BHLYP, and B3LYP).

Table 2. Performance of Different Exchange−Correlation Functionals for the Calculations of Core-Electron Binding Energies (BE) and K-Edge Energies (KE) of Molecular Compounds Containing the Elements C, O, N, and F[a]

	B3LYP		BHLYP		BLYP		PBE0		PBE		SCAN	
element	BE	KE	BE	KE	BE	KE	BE	KE	BE	KE	BE	KE
C	0.18	0.29	0.11	0.28	0.22	0.29	0.40	0.24	0.29	0.30	0.15	0.38
O	0.23	0.32	0.25	0.23	0.31	0.30	0.50	0.48	0.62	0.52	0.21	0.32
N	0.25	0.40	0.18	0.26	0.14	0.26	0.38	0.38	0.48	0.26	0.16	0.16
F	0.10	0.10	0.30	0.10	0.10	0.30	0.40	0.40	0.00	0.40	0.00	0.10
average	0.24	0.31	0.19	0.25	0.23	0.31	0.42	0.36	0.42	0.39	0.16	0.33

[a]The mean absolute errors (MAEs) in eV are shown. For the core-electron binding energy calculations, the data sets consist of 9 (C), 6 (O), 5 (N), and 1 (F) different binding energies. For the K-edge energies, the data sets consist of 11 (C), 5 (O), 5 (N), and 1 (F) energies.

https://doi.org/10.1021/acs.jctc.2c00817
J. Chem. Theory Comput. 2022, 18, 7620−7629

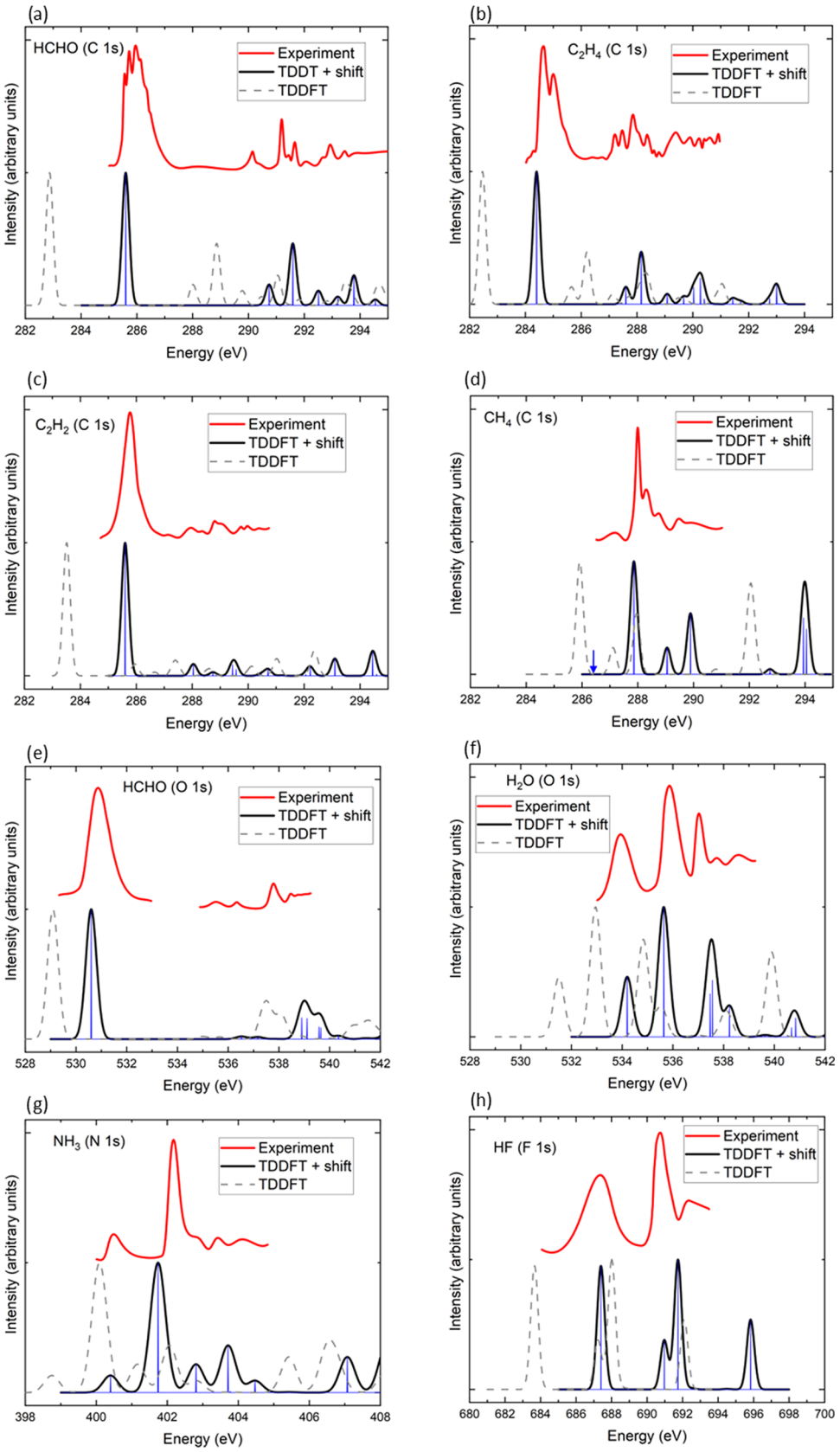

Figure 4. Comparison of calculated and experimental core-electron spectra for a set of small molecules. The BHLYP TDDFT spectra without the BHLYP ΔSCF shift are shown as faint dashed lines. The blue arrow in the CH_4 spectrum indicates the position of the electric-dipole forbidden excitation, which is visible in the experimental spectrum because of vibrational effects.

https://doi.org/10.1021/acs.jctc.2c00817
J. Chem. Theory Comput. 2022, 18, 7620−7629

Table 3. Core-Electron Binding Energies of Molecules Obtained from ΔSCF[a]

molecule	atom	exp.	B3LYP	BHLYP	BLYP	PBE0	PBE	SCAN
CH_4	C	290.7	290.7	290.6	290.6	290.5	290.7	290.7
NH_3	N	405.6	405.6	405.9	405.6	405.7	405.5	405.5
H_2O	O	539.7	539.7	539.5	539.4	539.5	539.6	539.6
HF	F	694.1	694.2	694.4	694.2	694.5	694.1	694.1
OCS	C	295.2	295.3	295.3	295.1	295.0	295.0	295.0
	O	540.3	540.2	540.6	540.1	539.6	539.3	540.3
CO	C	296.2	296.7	296.3	296.5	295.5	295.7	296.5
	O	542.1	542.4	542.4	542.6	541.7	541.7	542.6
acetone	$C(H_3)$	291.2	291.2	291.4	291.5	291.9	291.8	291.4
	C(O)	293.9	293.8	293.9	293.9	294.0	294.1	294.1
	O	537.9	537.5	537.8	537.5	537.0	536.7	537.6
C_2H_4	C	290.6	290.9	290.8	290.9	291.3	291.0	290.8
C_2H_2	C	291.2	291.4	291.5	291.7	291.8	291.6	291.3
formaldehyde	C	294.5	294.5	294.6	294.8	294.8	294.7	294.5
		539.0	539.3	539.5	539.7	539.7	539.8	539.3
ethanol	$C(H_2OH)$	291.1	290.9	291.1	291.3	291.3	291.4	290.9
	$C(H_3)$	292.5	292.1	292.5	292.6	292.8	292.6	292.4
	O	538.6	538.2	539.0	538.6	538.1	537.9	538.6
pyridine	N	404.9	404.5	404.8	404.9	405.2	405.2	404.6
pyridazine	N	404.9	405.2	405.2	405.3	405.3	405.3	404.7
pyrimidine	N	405.2	404.6	405.3	405.5	405.7	405.8	405.0
pyrazine	C	291.7	291.4	291.4	291.6	291.7	291.6	291.5
	N	405.6	405.2	405.5	405.6	406.2	406.6	405.6
MAE			0.2	0.2	0.2	0.4	0.4	0.2

[a]All energies are given in eV.

Table 4. K-Edge Energies of Molecules Obtained from ΔSCF[a]

molecule	atom	experiment	B3LYP	BHLYP	BLYP	PBE0	PBE	SCAN
CH_4	C	286.8	286.4	286.5	286.6	286.7	286.8	286.4
NH_3	N	400.4	399.9	400.4	400.5	400.6	400.6	400.5
H_2O	O	533.9	534.5	534.2	534.2	534.6	534.7	534.2
HF	F	687.3	687.4	687.4	687.6	687.7	687.7	687.4
OCS	C	288.4	287.6	287.6	287.6	287.8	287.7	287.8
	O	533.1	533.3	533.2	533.5	532.8	532.7	533.5
CO	C	287.3	287.4	287.2	287.3	287.4	287.4	286.4
	O	533.1	533.6	533.3	533.5	533.9	534.0	533.8
Acetone	$C(H_3)$	286.4	286.8	286.8	286.9	287.0	287.0	286.8
	O	530.7	530.6	531.0	531.0	530.1	530.2	530.7
C_2H_4	C	284.4	284.2	284.3	284.3	284.3	284.4	284.2
C_2H_2	C	285.6	285.6	285.1	286.0	285.8	285.4	285.1
Formaldehyde	C	285.6	285.4	285.4	285.5	285.7	285.8	285.4
	O	530.8	530.6	530.6	530.7	530.8	530.8	530.6
Ethanol	$C(H_2OH)$	286.9	287.0	287.0	287.1	287.2	287.3	287.0
	O	532.6	***	***	533.4	533.6	534.1	533.6
Pyridine	C	284.9	284.2	284.4	284.3	284.8	284.6	284.5
	N	398.8	398.3	398.4	398.5	398.6	398.7	398.7
Pyridazine	C	285.5	285.8	285.6	285.7	285.8	285.8	285.8
	N	399.0	398.8	398.9	399.0	399.1	399.1	399.1
Pyrimidine	C	284.9	285.0	285.1	285.3	285.3	285.7	285.1
	N	398.8	398.2	398.3	398.4	398.4	398.5	398.5
Pyrazine	C	285.3	285.1	285.3	285.3	285.3	285.3	285.0
	N	398.8	399.0	399.1	399.3	399.8	399.4	399.0
MAE			0.3	0.3	0.3	0.4	0.4	0.3

[a]All energies are given in eV. For excitations from O 1s in ethanol, results could not be obtained for B3LYP and BHLYP because of variational collapse problems (indicated by ***).

however, that the first low-intensity peak in the experimental spectrum at 287.05 eV arises from a transition from the carbon 1s orbital to 3s a_1 Rydberg orbital. This transition is electric-dipole-forbidden and only observable because of vibrational coupling. The largest peak at 288.0 eV arises from a transition into the 3p t_2 Rydberg state and is followed by smaller peaks

https://doi.org/10.1021/acs.jctc.2c00817
J. Chem. Theory Comput. 2022, 18, 7620−7629

arising from vibrational effects. At higher energies, additional peaks arising from transitions into higher Rydberg states are observed. In the calculated spectrum, the energy of the largest peak is underestimated, but better agreement is found for the higher-lying Rydberg state transitions.

Figure 4e,f shows the measured[38,51] and calculated oxygen spectra of H_2O and CH_2O. For H_2O, very good agreement between theory and experiment is found for both the peak positions and their intensities. The first two peaks arise from transitions from oxygen 1s to the $4a_1$ LUMO and $2b_2$ LUMO + 1 orbitals, respectively, while the final state of the third peak is a Rydberg state. Vibrational effects are responsible for the large width of the peaks. For CH_2O, the measured spectrum consists of a large peak at about 530.8 eV, which is well reproduced by theory, and a series of smaller peaks arising from transitions into Rydberg states, which are captured by the calculations. In particular, the calculated spectrum also exhibits two small peaks near 537 eV, which arise from transitions into 3s and 3p Rydberg states followed by two somewhat larger peaks near 539 eV corresponding to transitions into 4p and 5p Rydberg states. However, the energies of these smaller peaks are approximately 1 eV higher in the calculated spectrum compared to that in experiment.

Finally, Figure 4g,h shows the nitrogen spectrum of NH_3 and the fluorine spectrum of HF, respectively, and compares them to experimental XAS results.[38] Good agreement between theory and experiment is found for NH_3. In particular, the position and intensity of the first peak are well reproduced, but the energy of the large second peak near 402 eV is somewhat underestimated by the calculation. Similarly, the first peak at 687 eV in the HF spectrum is captured accurately by the calculation. At higher energies, near 692 eV, the theoretical spectra exhibit two peaks. In contrast to experiment, however, the intensity of the first peak is higher than that of the second peak.

CONCLUSIONS

We have assessed the performance of a first-principles approach for calculating core-electron spectra, which are measured in X-ray absorption spectroscopy and energetic electron loss spectroscopy. In this approach, spectra from linear-response TDDFT are shifted such that the energy of the lowest excitation agrees with the value obtained from ΔSCF. This procedure overcomes TDDFT's failure to yield accurate absolute core-electron excitation energies while producing the entire spectrum in one shot (as opposed to having a separate calculation for each excited state). We apply this method to a set of small molecules and find mostly good agreement between experimental and calculated spectra when the BHLYP exchange−correlation functional is used for the TDDFT. This method can now be applied to more complex systems, including solids and surfaces.

APPENDIX

Table 3 shows ΔSCF results for the binding energies for all molecules investigated in this study, and Table 4 shows the K-edge energies. Experimental values are taken from ref 38 for CH_4, H_2O, NH_3, and HF; ref 52 for ethanol, acetone, CO, and OCS; ref 51 for formaldehyde; ref 53 for C_2H_2 and C_2H_4; and ref 54 for pyridine, pyridazine, pyrimidine, and pyrazine.

ASSOCIATED CONTENT

Supporting Information

The Supporting Information is available free of charge at https://pubs.acs.org/doi/10.1021/acs.jctc.2c00817.

Relaxed atomic positions of all molecules studied in this paper (PDF)

AUTHOR INFORMATION

Corresponding Author

Johannes Lischner − *Departments of Materials, Imperial College London, London SW7 2AZ, United Kingdom; The Thomas Young Centre for Theory and Simulation of Materials, Imperial College London, London SW7 2AZ, United Kingdom;* orcid.org/0000-0002-9601-7821; Email: j.lischner@imperial.ac.uk

Authors

Marcus Annegarn − *Departments of Materials, Imperial College London, London SW7 2AZ, United Kingdom; The Thomas Young Centre for Theory and Simulation of Materials, Imperial College London, London SW7 2AZ, United Kingdom*

Juhan Matthias Kahk − *Institute of Physics, University of Tartu, 50411 Tartu, Estonia;* orcid.org/0000-0002-4873-7541

Complete contact information is available at: https://pubs.acs.org/10.1021/acs.jctc.2c00817

Notes

The authors declare no competing financial interest.

ACKNOWLEDGMENTS

J.L. acknowledges funding from the Royal Society through a Royal Society University Research Fellowship. This project has received funding from the European Union's Horizon 2020 research and innovation programme under grant agreement no. 892943. J.M.K. acknowledges support from the Estonian Centre of Excellence in Research project "Advanced materials and high-technology devices for sustainable energetics, sensorics and nanoelectronics" TK141 (2014-2020.4.01.15-0011). This work used the ARCHER2 UK National Supercomputing Service via J.L.'s membership of the HEC Materials Chemistry Consortium of UK, which is funded by EPSRC (EP/L000202).

REFERENCES

(1) Diller, K.; Maurer, R. J.; Müller, M.; Reuter, K. Interpretation of X-ray absorption spectroscopy in the presence of surface hybridization. *J. Chem. Phys.* **2017**, *146*, No. 214701.

(2) Abbehausen, C.; De Paiva, R. E. F.; Bjornsson, R.; Gomes, S. Q.; Du, Z.; Corbi, P. P.; Lima, F. A.; Farrell, N. X-ray Absorption Spectroscopy Combined with Time-Dependent Density Functional Theory Elucidates Differential Substitution Pathways of Au(I) and Au(III) with Zinc Fingers. *Inorg. Chem.* **2018**, *57*, 218−230.

(3) Zhovtobriukh, I.; Norman, P.; Pettersson, L. G. X-ray absorption spectrum simulations of hexagonal ice. *J. Chem. Phys.* **2019**, *150*, 363−370.

(4) Cavalleri, M.; Ogasawara, H.; Pettersson, L. G.; Nilsson, A. interpretation of X-ray absorption spectra of water and ice. *Chem. Phys. Lett.* **2002**, *364*, 363−370.

(5) Datta, S.; Rule, A. M.; Mihalic, J. N.; Chillrud, S. N.; Bostick, B. C.; Ramos-Bonilla, J. P.; Han, I.; Polyak, L. M.; Geyh, A. S.; Breysse, P. N. Use of X-ray absorption spectroscopy to speciate manganese in

airborne particulate matter from five counties across the United States. *Environ. Sci. Technol.* **2012**, *46*, 3101−3109.
(6) Chen, Y.; Shah, N.; Braun, A.; Huggins, F. E.; Huffman, G. P. Electron microscopy investigation of carbonaceous particulate matter generated by combustion of fossil fuels. *Energy Fuels* **2005**, *19*, 1644−1651.
(7) Casida, M. E.*Recent Advances In Density Functional Methods: (Part I)*; World Scientific, 1995; pp 155−192.
(8) Besley, N. A.; Asmuruf, F. A. Time-dependent density functional theory calculations of the spectroscopy of core electrons. *Phys. Chem. Chem. Phys.* **2010**, *12*, 12024−12039.
(9) Oosterbaan, K. J.; White, A. F.; Head-Gordon, M. Non-orthogonal configuration interaction with single substitutions for the calculation of core-excited states. *J. Chem. Phys.* **2018**, *149*, No. 044116.
(10) Besley, N. A.; Noble, A. Time-dependent density functional theory study of the X-ray absorption spectroscopy of acetylene, ethylene, and benzene on Si (100). *J. Phys. Chem. C* **2007**, *111*, 3333−3340.
(11) Norman, P.; Dreuw, A. Simulating X-ray spectroscopies and calculating core-excited states of molecules. *Chem. Rev.* **2018**, *118*, 7208−7248.
(12) Wenzel, J.; Wormit, M.; Dreuw, A. Calculating core-level excitations and X-ray absorption spectra of medium-sized closed-shell molecules with the algebraic-diagrammatic construction scheme for the polarization propagator. *J. Comput. Chem.* **2014**, *35*, 1900−1915.
(13) Attar, A. R.; Bhattacherjee, A.; Pemmaraju, C.; Schnorr, K.; Closser, K. D.; Prendergast, D.; Leone, S. R. Femtosecond X-ray spectroscopy of an electrocyclic ring-opening reaction. *Science* **2017**, *356*, 54−59.
(14) Bhattacherjee, A.; Schnorr, K.; Oesterling, S.; Yang, Z.; Xue, T.; de Vivie-Riedle, R.; Leone, S. R. Photoinduced heterocyclic ring opening of furfural: Distinct open-chain product identification by ultrafast X-ray transient absorption spectroscopy. *J. Am. Chem. Soc.* **2018**, *140*, 12538−12544.
(15) Besley, N. A.; Peach, M. J.; Tozer, D. J. Time-dependent density functional theory calculations of near-edge X-ray absorption fine structure with short-range corrected functionals. *Phys. Chem. Chem. Phys.* **2009**, *11*, 10350−10358.
(16) DeBeer George, S.; Petrenko, T.; Neese, F. Time-dependent density functional calculations of ligand K-edge X-ray absorption spectra. *Inorg. Chim. Acta* **2008**, *361*, 965−972.
(17) DeBeer George, S.; Neese, F. Calibration of scalar relativistic density functional theory for the calculation of sulfur K-edge X-ray absorption spectra. *Inorg. Chem.* **2010**, *49*, 1849−1853.
(18) Gilbert, A. T. B.; Besley, N. A.; Gill, P. M. Self-consistent field calculations of excited states using the maximum overlap method (MOM). *J. Phys. Chem. A* **2008**, *112*, 13164−13171.
(19) Kowalczyk, T.; Yost, S. R.; Voorhis, T. V. Assessment of the ΔSCF density functional theory approach for electronic excitations in organic dyes. *J. Chem. Phys.* **2011**, *134*, No. 054128.
(20) Ziegler, T.; Rauk, A.; Baerends, E. J. On the calculation of multiplet energies by the Hartree-Fock-Slater method. *Theor. Chim. Acta* **1977**, *43*, 261−271.
(21) Kahk, J. M.; Lischner, J. Core electron binding energies of adsorbates on Cu(111) from first-principles calculations. *Phys. Chem. Chem. Phys.* **2018**, *20*, 30403−30411.
(22) Kahk, J. M.; Lischner, J. Accurate absolute core-electron binding energies of molecules, solids, and surfaces from first-principles calculations. *Phys. Rev. Mater.* **2019**, *3*, No. 100801.
(23) Ambroise, M. A.; Jensen, F. Probing Basis Set Requirements for Calculating Core Ionization and Core Excitation Spectroscopy by the δ Self-Consistent-Field Approach. *J. Chem. Theory Comput.* **2019**, *15*, 325−337.
(24) Zhekova, H. R.; Seth, M.; Ziegler, T. A perspective on the relative merits of time-dependent and time-independent density functional theory in studies of the electron spectra due to transition metal complexes. An illustration through applications to copper tetrachloride and plastocyanin. *Int. J. Quantum Chem.* **2014**, *114*, 1019−1029.
(25) Hait, D.; Head-Gordon, M. Excited state orbital optimization via minimizing the square of the gradient: General approach and application to singly and doubly excited states via density functional theory. *J. Chem. Theory Comput.* **2019**, *16*, 1699−1710.
(26) Hait, D.; Head-Gordon, M. Highly Accurate Prediction of Core Spectra of Molecules at Density Functional Theory Cost: Attaining Sub-electronvolt Error from a Restricted Open-Shell Kohn-Sham Approach. *J. Phys. Chem. Lett.* **2020**, *11*, 775−786.
(27) Tait, E. W.; Ratcliff, L. E.; Payne, M. C.; Haynes, P. D.; Hine, N. D. Simulation of electron energy loss spectra of nanomaterials with linear-scaling density functional theory. *J. Phys.: Condens. Matter* **2016**, *28*, No. 195202.
(28) Morris, A. J.; Nicholls, R. J.; Pickard, C. J.; Yates, J. R. OptaDOS: A tool for obtaining density of states, core-level and optical spectra from electronic structure codes. *Comput. Phys. Commun.* **2014**, *185*, 1477−1485.
(29) Coriani, S.; Christiansen, O.; Fransson, T.; Norman, P. Coupled-cluster response theory for near-edge X-ray-absorption fine structure of atoms and molecules. *Phys. Rev. A: At., Mol., Opt. Phys.* **2012**, *85*, No. 022507.
(30) Mizoguchi, T.; Tanaka, I.; Yoshiya, M.; Oba, F.; Ogasawara, K.; Adachi, H. Core-hole effects on theoretical electron-energy-loss near-edge structure and near-edge X-ray absorption fine structure of MgO. *Phys. Rev. B: Condens. Matter Mater. Phys.* **2000**, *61*, 2180.
(31) Kehry, M.; Franzke, Y. J.; Holzer, C.; Klopper, W. Quasirelativistic two-component core excitations and polarisabilities from a damped-response formulation of the Bethe-Salpeter equation. *Mol. Phys.* **2020**, *118*, No. e1755064.
(32) Gilmore, K.; Vinson, J.; Shirley, E. L.; Prendergast, D.; Pemmaraju, C. D.; Kas, J. J.; Vila, F. D.; Rehr, J. J. Efficient implementation of core-excitation Bethe-Salpeter equation calculations. *Comput. Phys. Commun.* **2015**, *197*, 109−117.
(33) Zheng, C.; Mathew, K.; Chen, C.; Chen, Y.; Tang, H.; Dozier, A.; Kas, J. J.; Vila, F. D.; Rehr, J. J.; Piper, L. F.; Persson, K. A.; Ong, S. P. Automated generation and ensemble-learned matching of X-ray absorption spectra. *npj Comput. Mater.* **2018**, *4*, No. 12.
(34) Torrisi, S. B.; Carbone, M. R.; Rohr, B. A.; Montoya, J. H.; Ha, Y.; Yano, J.; Suram, S. K.; Hung, L. Random forest machine learning models for interpretable X-ray absorption near-edge structure spectrum-property relationships. *npj Comput. Mater.* **2020**, *6*, No. 109.
(35) Aarva, A.; Deringer, V. L.; Sainio, S.; Laurila, T.; Caro, M. A. Understanding X-ray Spectroscopy of Carbonaceous Materials by Combining Experiments, Density Functional Theory, and Machine Learning. Part I: Fingerprint Spectra. *Chem. Mater.* **2019**, *31*, 9243−9255.
(36) Rankine, C. D.; Madkhali, M. M.; Penfold, T. J. A Deep Neural Network for the Rapid Prediction of X-ray Absorption Spectra. *J. Phys. Chem. A* **2020**, *124*, 4263−4270.
(37) Leetmaa, M.; Ljungberg, M.; Ogasawara, H.; Odelius, M.; Näslund, L.-Å.; Nilsson, A.; Pettersson, L. G. Are recent water models obtained by fitting diffraction data consistent with infrared/Raman and X-ray absorption spectra? *J. Chem. Phys.* **2006**, *125*, No. 244510.
(38) Nilsson, A.; Nordlund, D.; Waluyo, I.; Huang, N.; Ogasawara, H.; Kaya, S.; Bergmann, U.; Näslund, LÅ.; Öström, H.; Wernet, P.; Andersson, K. J.; Schiros, T.; Pettersson, L. G. X-ray absorption spectroscopy and X-ray Raman scattering of water and ice; an experimental view. *J. Electron Spectrosc. Relat. Phenom.* **2010**, *177*, 99−129.
(39) Blum, V.; Gehrke, R.; Hanke, F.; Havu, P.; Havu, V.; Ren, X.; Reuter, K.; Scheffler, M. Ab initio molecular simulations with numeric atom-centered orbitals. *Comput. Phys. Commun.* **2009**, *180*, 2175−2196.
(40) Ren, X.; Rinke, P.; Blum, V.; Wieferink, J.; Tkatchenko, A.; Sanfilippo, A.; Reuter, K.; Scheffler, M. Resolution-of-identity approach to Hartree-Fock, hybrid density functionals, RPA, MP2 and GW with numeric atom-centered orbital basis functions. *New J. Phys.* **2012**, *14*, No. 053020.

https://doi.org/10.1021/acs.jctc.2c00817
J. Chem. Theory Comput. 2022, 18, 7620−7629

(41) van Lenthe, E.; Baerends, E. J.; Snijders, J. G. Relativistic total energy using regular approximations. *J. Chem. Phys.* **1994**, *101*, 9783−9792.
(42) Faas, S.; Snijders, J. G.; van Lenthe, J. H.; van Lenthe, E.; Baerends, E. J. The ZORA formalism applied to the Dirac-Fock equation. *Chem. Phys. Lett.* **1995**, *246*, 632−640.
(43) Dyall, K. G.; van Lenthe, E. Relativistic regular approximations revisited: An infinite-order relativistic approximation. *J. Chem. Phys.* **1999**, *111*, 1366−1372.
(44) Klopper, W.; van Lenthe, J. H.; Hennum, A. C. An improved ab initio relativistic zeroth-order regular approximation correct to order 1/c2. *J. Chem. Phys.* **2000**, *113*, 9957−9965.
(45) Aprà, E.; Bylaska, E. J.; de Jong, W. A.; et al. NWChem: Past, present, and future. *J. Chem. Phys.* **2020**, *152*, No. 184102.
(46) Dunning, T. H. Gaussian basis sets for use in correlated molecular calculations. I. The atoms boron through neon and hydrogen. *J. Chem. Phys.* **1989**, *90*, 1007−1023.
(47) Kendall, R. A.; Dunning, T. H.; Harrison, R. J. Electron affinities of the first-row atoms revisited. Systematic basis sets and wave functions. *J. Chem. Phys.* **1992**, *96*, 6796−6806.
(48) Pritchard, B. P.; Altarawy, D.; Didier, B.; Gibsom, T. D.; Windus, T. L. A New Basis Set Exchange: An Open, Up-to-date Resource for the Molecular Sciences Community. *J. Chem. Inf. Model.* **2019**, *59*, 4814−4820.
(49) Feller, D. The role of databases in support of computational chemistry calculations. *J. Comput. Chem.* **1996**, *17*, 1571−1586.
(50) Schuchardt, K. L.; Didier, B. T.; Elsethagen, T.; Sun, L.; Gurumoorthi, V.; Chase, J.; Li, J.; Windus, T. L. Basis Set Exchange: A Community Database for Computational Sciences. *J. Chem. Inf. Model.* **2007**, *47*, 1045−1052.
(51) Remmers, G.; Domke, M.; Puschmann, A.; Mandel, T.; Xue, C.; Kaindl, G.; Hudson, E.; Shirley, D. A. High-resolution K-shell photoabsorption in formaldehyde. *Phys. Rev. A* **1992**, *46*, 3935−3944.
(52) Sham, T. K.; Yang, B. X.; Kirz, J.; Tse, J. S. K-edge near-edge X-ray-absorption fine structure of oxygen- and carbon-containing molecules in the gas phase. *Phys. Rev. A* **1989**, *40*, 652−669.
(53) Tronc, M.; King, G. C.; Read, F. H. Carbon K-shell excitation in small molecules by high-resolution electron impact. *J. Phys. B: At. Mol. Phys.* **1979**, *12*, 137−157.
(54) Vall-Llosera, G.; Gao, B.; Kivimäki, A.; Coreno, M.; Álvarez Ruiz, J.; De Simone, M.; Ågren, H.; Rachlew, E. The C 1s and N 1s near edge X-ray absorption fine structure spectra of five azabenzenes in the gas phase. *J. Chem. Phys.* **2008**, *128*, No. 044316.

https://doi.org/10.1021/acs.jctc.2c00817
J. Chem. Theory Comput. 2022, 18, 7620−7629